Vacuum deposition of $CsPbI_3$ layers on textured Si for perovskite/Si tandem solar cells

Keitaro Hamada[1*], Kyosuke Yonezawa[2], Kohei Yamamoto[2], Tetsuya Taima[2], Shuzi Hayase[3], Noboru Ooyagi[4], Yuzo Yamamoto[4], Keisuke Ohdaira[1]

[1]*Japan Advanced Institute of Science and Technology, 1-1 Asahidai, Nomi, Ishikawa 923-1292, Japan*

[2]*Kanazawa University, Kakuma, Kanazawa 920-1192 Japan*

[3]*Kyushu Institute of Technology, 1-1 Sensui-cho, Tobata-ku, Kitakyushu-shi, Fukuoka, 804-8550, Japan*

[4]*Settsu Oil Mill, 1-5-10 Chikkoshinmachi, Nishi-ku Sakai-shi, Osaka, 592-8331, Japan*

[*]E-mail: ohdaira@jaist.ac.jp

We attempt the conformal deposition of $CsPbI_3$ layers on pyramidal-shaped textured crystalline Si (c-Si) surfaces, aiming at application to Perovskite/Si tandem solar cells. $CsPbI_3$ layers are deposited through vacuum evaporation on textured c-Si surfaces with various pyramid sizes. Conformal $CsPbI_3$ layers are formed on the texture c-Si, which is, in principle, difficult to be realized by conventional solution process. We also confirmed a reduction in the optical reflectance of $CsPbI_3$/Si structures by ~10% (absolute) by using textured c-Si compared to the case of flat Si. A co-evaporation method can prevent the aggregation of CsI particles, which are seen when the films are formed by sequential evaporation. These results indicate the feasibility of Perovskite/c-Si tandem cells with textured c-Si, leading to low optical reflectivity and high photocurrent.

1. Introduction

Perovskite solar cells such as organic-inorganic Perovskite $CH_3NH_3PbI_3$ have been attracting attention as high-efficiency thin-film solar cells, because they show a dramatic improvement of power conversion efficiency (PCE) from 3.8[1)] to 23.3%[2)] in only 9 years from the first report in 2009. Perovskite/Si tandem solar cells are one of the solutions to overcome the PCE of crystalline silicon (c-Si) solar cells, which have been widely used and dominated the present share of photovoltaic market. The currently reported maximum PCE of the c-Si cells is 26.7%[3)], closely approaching the Shockley-Queisser (S-Q) limit[4)] of 29.4%[5)]. Perovskite/Si tandem solar cells can improve the S-Q limit up to 40.6%[6)]. Several Perovskite/Si tandem solar cells have been recently reported, and the present maximum PCEs of 4-terminal and 2-terminal (monolithic) Perovskite/Si tandem solar cells are 27.1%[7)] and 27.3%[8)], respectively. To reach the PCE more than the theoretical limit of c-Si, it is necessary to optimize the fabrication process of the Perovskite solar cells on c-Si.

Perovskite solar cells used for the top cells of tandem solar cells are generally produced by solution processes such as spin coating.[9)] However, the solution processes require the wettability and smoothness of the underlying surface of substrates. c-Si solar cells generally have micrometer-order pyramidal-shaped texture structures on both sides of c-Si wafers for effective light trapping.[10,11)] The surface textures on c-Si will contribute to a reduction in the optical reflectance also in the case of Perovskite/Si tandem solar cells, and the Perovskite layers are required to be conformally formed on the pyramids. The unevenness on the textured c-Si surface of several μm, however, causes solution pooling in the valleys between the pyramids. This makes it difficult to form thin films that conformally cover the surfaces of c-Si pyramids. Only flat Si wafers have therefore been used in the solution process, and the PCE of the tandem cells is limited by the reflection loss due to the insufficient antireflection.[12–14)] If the Perovskite films are formed by vacuum deposition, the problem of the pooling of Perovskite materials will be solved. Although there have been several reports for the conformal formation of Perovskite films on textured Si, they partially includes solution process.[15,16)] The formation of Perovskite layers only through the vacuum process may be preferable in the future mass-production of the Perovskite/Si tandem cells.

In this study, vacuum evaporation has been applied for a new method to deposit $CsPbI_3$ Perovskite layers on textured Si, instead of the conventional solution process. We have so

far reported the stable formation of fully inorganic Perovskite $CsPbI_3$ films without gasification by vacuum evaporation and the application of the $CsPbI_3$ films to a solar cell absorber.[17, 18] $CsPbI_3$ has also been reported as having highly efficient optical and electrical properties.[19–27] The currently reported maximum PCE of the $CsPbI_3$ cells is 13.5%.[28] The vacuum deposition of thin films can realize, in general, high step coverage and can control the thickness of films precisely. We expect that these properties can be utilized for the conformal formation of Perovskite films on micrometer-sized Si pyramids. We have thus prepared Si wafers with texture structures with different sizes, and evaporated $CsPbI_3$ films thereon to verify the formation of continuous films with good uniformity and coverage. Moreover, to verify the antireflection effect by the usage of textured c-Si wafers, we compared optical reflectance spectra after the formation of the $CsPbI_3$ films on flat and textured c-Si and estimated an increase in photocurrent, as partly reported in our previous work.[29] We have also compared with sequential and co-evaporation to determine a better method for the conformal deposition of $CsPbI_3$ films.

2. Experimental methods

We used 290-μm-thick mirror-polished floating-zone-grown n-type Si(100) wafers with a resistivity of 1–5 Ωcm. After cleaning the wafers in ozone water for 5 minutes, alkali anisotropic etching was performed using two types of etching solutions with different additives (SE-2000H, SUN-X 600) to form pyramidal-shaped textures. The c-Si wafers were immersed in the etching solutions under the conditions shown in Table I. The textured wafers were then ultrasonically cleaned in deionized water for 15 minutes. We observed the surfaces of the textured Si wafers by scanning electron microscopy (SEM) and evaluated the size of pyramids.

Figure 1 shows the surface SEM images of textured Si wafers after alkali etching. Table I shows the heights of the pyramidal-shaped textures measured from Fig. 1. Textures with different sizes were obtained depending on etching solutions and conditions, which are indicated as [S], [M], and [L]. The surface image of [S] shows flat gaps, probably with (100) orientation, on the surface between the pyramids. On the contrary, there are no such gaps on the images of [M] and [L]. [L] has a larger average size of pyramids than [M].

Figure 2 shows the reflectance spectra of the textured and flat Si wafers. Table II shows

average reflectance (R_{AVE}) calculated from Fig. 2 spectra in a wavelength range of 400 to 800 nm. The optical reflectance was reduced, compared to flat Si, by the formation of pyramidal-shaped textures formed under any conditions. [M] shows 15% (absolute) lower reflectance than a flat wafer. The textured surface reduces the optical reflection by the multiple reflection effect of reflected light being incident again on adjacent pyramids with Si(111) facets. [S] shows worse antireflection ability, which is probably due to remaining Si(100) in the gap. [L] shows higher reflectance than [M], which may be due to less uniform pyramid sizes.

We next formed $CsPbI_3$ layers on the textured Si wafers through two types of evaporation processes: sequential evaporation and co-evaporation. In the sequential evaporation, 150-nm-thick PbI_2 and 80-nm-thick CsI were evaporated in this order on the textured Si substrates at a pressure of 2.0×10^{-4} Pa. Small amounts of PbI_2 and CsI powders were placed in a K-cell with a diameter of 5 cm and a depth of 1.2 cm and a tungsten boat, respectively, inside the chamber and carefully heated to allow outgassing. The K-cell was heated at 420 °C, resulting in a growth rate of 0.5 Å/s for PbI_2. The tungsten boat was electrically heated so that the growth rate of CsI was 0.3 Å/s. The thickness and growth rate were monitored with a quartz crystal oscillator. The K-cell and the tungsten boat were 30 and 35 cm from the substrates, respectively. In the co-evaporation, PbI_2 and CsI were evaporated simultaneously on the textured Si substrates at deposition rates of 0.5 and 0.3 Å/s for 50 min. These samples were then annealed at 350 °C for 1 minute on a hot plate to form $CsPbI_3$ layers. We prepared $CsPbI_3$ layers also on flat c-Si wafers in the same ways. The coverage of $CsPbI_3$ layers on flat and textured c-Si wafers was confirmed from the cross-sectional scanning electron microscope (SEM) images. The element distribution in the films was analyzed by energy dispersive X-ray spectroscopy (EDX).

PbI_2 films were formed on the texture Si also by a solution method for comparison to confirm that the conformal film formation by solution process is actually difficult. Textured Si wafers first received oxygen plasma treatment for 20 min. PbI_2 precursor solutions (230 mg/ml in N, N-dimethylformamide) stirred for >12 hours were then spin-coated on the textured Si wafers at 2000 rpm for 60 sec, followed by annealing at 100 ºC for 10 min.

We measured the reflectance spectra of the $CsPbI_3$/c-Si stacks using an ultraviolet-visible spectrophotometer (UV-vis) to compare reflection losses of the samples with flat and

textured Si wafers on which $CsPbI_3$ films were formed. Based on these results, we estimated an increase in photocurrent under the assumption that all the absorbed photons generate carriers and all the carriers are collected as a current. We evaluated, from the reflectance (R) data, how much short-circuit current density (J_{SC}) increases in Perovskite/Si tandem solar cells by the utilization of textured c-Si using the following eq. (1).

$$J_{sc} = q \int_{300}^{1200} N_{Photon(AM1.5G)} \cdot (1 - R)\, d\lambda \qquad (1)$$

3. Results and discussion

3.1 Sequential evaporation of $CsPbI_3$

Figure 3 shows the cross-sectional SEM image of a PbI_2 film formed on textured Si by the solution process described in the previous section. Despite the improved wettability of the surface by the oxygen plasma treatment, spin-coated PbI_2 is aggregated and crystallized in the valleys between pyramids in the form of a liquid pool, while the top of the pyramids are covered with a PbI_2 film. This clearly indicates that the difficulty of conformally forming a perovskite film on micrometer-sized pyramids by a solution method.

We next carried out the vacuum evaporation of $CsPbI_3$ layers on the textured Si wafers with three types of pyramids: [S], [M] and [L]. Figure 4 shows the cross-sectional SEM images of $CsPbI_3$ layers deposited through sequential evaporation on the three types of textured wafers as well as on a flat Si wafer. The conformal formation of $CsPbI_3$ layers can be seen for all the pyramidal-shaped c-Si surfaces, regardless of the size of pyramids. These results indicate that it is possible to form $CsPbI_3$ layers with good uniformity and coverage on textured Si wafers by sequential evaporation, unlike in the case of conventional solution process. One can see protrusions in the $CsPbI_3$ films formed on textured c-Si particularly at the tips of the pyramids. Similar structures are seen also in the film formed on a flat c-Si wafer. These may originate from aggregated excess Cs. We confirmed the formation of an impurity crystals of Cs_4PbI_6 by X-ray diffraction (XRD) in our previous studies [17,18].

Figure 5 shows the optical reflectance spectra of three types of textured Si and flat Si coated with $CsPbI_3$ layers. A broad peak at a wavelength of ~800 nm due to optical interference is seen only in the spectrum for the flat Si sample. Average reflectance (R_{AVE}) in a wavelength region of 400–800 nm are summarized in Table III. All the $CsPbI_3$ films

formed on textured Si showed R_{AVE} of ~10% (absolute) lower than that of $CsPbI_3$ films on the flat wafer. This suggests that reflection loss on the $CsPbI_3$ surface can be greatly reduced by using textured Si. Note that R_{AVE} for the samples with textured Si wafers is almost independent of the size of pyramids. This means that low optical reflectance can be obtained on textured Si surfaces with any sizes.

To estimate maximum J_{SC} gain by the usage of textured Si, we assumed that all the unreflective photons are absorbed and produce photocurrent with 100% internal quantum efficiency, and the two sub-cell, $CsPbI_3$ and c-Si, produce the same current. J_{SC} for the flat and [M] size textured wafers were estimated to be 19.3 and 21.5 mA/cm^2, respectively. This means that J_{SC} can be improved by ~2 mA/cm^2 by using textured Si, which is a great benefit for the Perovskite/Si tandem cells.

3.2 Comparison of sequential and co-evaporations

Figure 6 shows the cross-sectional SEM images of sequentially evaporated $CsI/PbI_2/Si$ stacks before annealing for crystallization. We see two kinds of layers on the textured Si: (a) thin layers formed conformally on the pyramids, which appear gray in the image, and (b) columnar structures, which appear white, standing perpendicularly on the conformal layer. According to the order of sequential evaporation, these are identified to be PbI_2 and CsI, respectively. The formation of columnar CsI might be due to poor sticking probability and/or insufficient migration on PbI_2.[30] Once CsI columns are formed, they will grow selectively due to the self-projection effect, which may occur especially at protrude parts—the top of the pyramids.

Figure 7 shows the cross-sectional SEM and EDX mapping images of sequentially evaporated $CsI/PbI_2/Si$ stacks before annealing and $CsPbI_3/Si$ stacks after annealing. Cs is intensely detected particularly at the tops of pyramids before annealing, probably originating from columnar CsI. We still see strong Cs signals at the top of the pyramids even after annealing. This indicates that the aggregated Cs before annealing remains and the Cs-rich impurity phase of Cs_4PbI_6 may be formed. In addition, Cs accumulation is partly confirmed also on Si(111) facets. From these results, we conclude that $CsPbI_3$ layers formed by sequential evaporation tend to contain a large amount of the impurity phase of Cs_4PbI_6, which is attributable to the localization of CsI due to the columnar growth.

Since it is difficult to uniformly deposit CsI on PbI_2 films, attempts were made to solve the aggregation of CsI by using co-evaporation, instead of sequential evaporation. Figure 8 shows the cross-sectional SEM and EDX mapping images of co-evaporated (CsI)(PbI_2)/Si stacks before annealing and $CsPbI_3$/Si stacks after annealing. The coverage of the (CsI)(PbI_2) mixed film before annealing is greatly improved compared to the case of sequential evaporation, and no significant element localization is observed. This also affect the structure of the final $CsPbI_3$ films after annealing. We see no clear localization of Cs-rich regions even at the tops of the pyramids. We thus consider that by using co-evaporation, the uniform distribution of CsI and continuous film formation are realized. Unlike in the case of sequential evaporation, two kinds of materials are supplied simultaneously on a Si surface in the co-evaporation. The migration of CsI for the uniform composition is thus less significant than in the case of sequential evaporation. Other critical difference between the two evaporation methods is that CsI is deposited on PbI_2 in the sequential evaporation, while it is evaporated directly on a c-Si surface in the early stage and then on a (CsI)(PbI_2) mixed film surface thereafter. This might affect the sticking probability of CsI and the suppression of columnar structures.

We should finally emphasize that the method of conformally forming Perovskite films on textured Si proposed in this study does not include any solution processes at all, unlike in the case of previous studies. This will contribute to the development of industrialized process for Perovskite/Si tandem cells.

4. Conclusions

The vacuum deposition of $CsPbI_3$ films can realize good coverage on pyramidal-shaped c-Si textures, which is difficult by the conventional solution process. The conformal formation of $CsPbI_3$ films can be seen independent of pyramid size. The utilization of textured Si leads to a reduction in optical reflectance by ~10% (absolute), corresponding to an improvement in J_{sc} of ~2 mA/cm^2 in Perovskite/Si tandem cells. Co-evaporation suppresses columnar growth and aggregation of CsI at the top of pyramids. These demonstrate the possibility of realizing new fabrication processes for perovskite/Si tandem solar cells using textured Si.

References

1) A. Kojima, K. Teshima, Y. Shirai and T. Miyasaka, J. Am. Chem. Soc. **131**, 6050 (2009).
2) NREL Efficiency Chart (NREL, 2018).
3) K. Yamamoto, K. Yoshikawa, H. Uzu, and D. Adachi, Jpn. J. Appl. Phys. **57**, 08RB20 (2018).
4) W. Shockley and H. J. Queisser, J. Appl. Phys. **32**, 510 (1961).
5) A. Richter, M. Hermle, and S. W. Glunz, IEEE J. Photovoltaics **3**, 1184 (2013).
6) I. Almansouri, A. Ho-Baillie, and M. A. Green, Jpn. J. Appl. Phys. **54**, 08KD04 (2015).
7) https://www.pv-tech.org/news/imec-pushes-4-terminal-perovskite-silicon-tandem-solar-cell-to-record-27.1
8) https://www.oxfordpv.com/news/oxford-pv-sets-world-record-perovskite-solar-cell
9) W. S. Yang, B. W. Park, E. H. Jung, N. J. Jeon, Y. C. Kim, D. U. Lee, S. S. Shin, J. Seo, E. K. Kim, J. H. Noh, and S. I. Seok, Science **356**, 6345 (2017).
10) D. L. King and M. E. Buck, 22nd IEEE Photovoltaics Specialists Conf. **1**, 303 (1991).
11) M. J. Declercq, L. Gerzberg and J. D. Meindl, J. Electrochem. Soc. **122**, 545 (1975).
12) S. Albrecht, M. Saliba, J. Pablo C. Baena, F. Lang, L. Kegelmann, M. Mews, L. Steier, A. Abate, J. Rappich, L. Korte, R. Schlatmann, M. K. Nazeeruddin, A. Hagfeldt, M. Grätzeld and B. Recha, Energy Environ. Sci. **9**, 81 (2016).
13) Z. Qiu, Z. Xu, N. Li, N. Zhou, Y. Chen, X. Wan, J. Liu, N. Li, X. Hao, P. Bi, Q. Chen, B. Cao and H. Zhou, Nano Energy **53**, 798 (2018).
14) R. Fan, N. Zhou, L. Zhang, R. Yang, Y. Meng, L. Li, T. Guo, Y. Chen, Z. Xu, G. Zheng, Y. Huang, L. Li, L. Qin, X. Qiu, Q. Chen, and H. Zhou, Sol. RRL **1**, 1700149 (2017).
15) F. Sahli, J. Werner, B. A. Kamino, M. Bräuninger, R. Monnard, B. Paviet-Salomon, L. Barraud, L. Ding, J. J. D. Leon, D. Sacchetto, G. Cattaneo, M. Despeisse, M. Boccard, S. Nicolay, Q. Jeangros, B. Niesen and C. Ballif, Nat. Mater. **17**, 820 (2018).
16) I. Raifuku, Y. Ishikawa, T. Bourgeteau, Y. Bonnassieux, P. R. i Cabarrocas and Y. Uraoka, Appl. Phys. Express **10**, 094101 (2017).
17) Md. Shahiduzzaman, K. Yonezawa, K. Yamamoto, T. S. Ripolles, M. Karakawa, T. Kuwabara, K. Takahashi, S. Hayase, and T. Taima, ACS Omega **2**, 4464 (2017).
18) K. Yonezawa, K. Yamamoto, Md. Shahiduzzaman, Y. Furumoto, K. Hamada, T. S. Ripolles, M. Karakawa, T. Kuwabara, K. Takahashi, and S. Hayase, Jpn. J. Appl. Phys. **56**, 04CS11

(2017).
19) D. M. Trots and S. V. Myagkota, J. Phys. Chem. Solids **69**, 2520 (2008).
20) G. Murtaza and I. Ahmad, Physica B **406**, 3222 (2011).
21) L. Protesescu, S. Yakunin, M. I. Bodnarchuk, F. Krieg, R. Caputo, C. H.Hendon, R. X. Yang, A. Walsh, and M. V. Kovalenko, Nano Lett. **15**, 3692 (2015).
22) D. Zhang, S. W. Eaton, Y. Yu, L. Dou, and P. Yang, J. Am. Chem. Soc. **137**, 9230 (2015).
23) G. E. Eperon, G. M. Paternò, R. J. Sutton, A. Zampetti, A. A. Haghighirad, F. Caciallibc, and H. J. Snaith, J. Mater. Chem. A **3**, 19688 (2015).
24) T. S. Ripolles, K. Nishinaka, Y. Ogomi, Y. Miyata, and S. Hayase, Sol. Energy Mater. Sol. Cells **144**, 532 (2016).
25) R. J. Sutton, G. E. Eperon, L. Miranda, E. S. Parrott, B. A. Kamino, J. B. Patel, M. T. Hörantner, M. B. Johnston, A. A. Haghighirad, D. T. Moore, and H. J. Snaith, Adv. Energy Mater. **6**, 1502458 (2016).
26) S. Yakunin, L. Protesescu, F. Krieg, M. I. Bodnarchuk, G. Nedelcu, M. Humer, G. D. Luca, M. Fiebig, W. Heiss, and M. V. Kovalenko, Nat. Commun. **6**, 8056 (2015).
27) M. Kulbak, S. Gupta, N. Kedem, I. Levine, T. Bendikov, G. Hodes, and D. Cahen, J. Phys. Chem. Lett. **7**, 167 (2016).
28) Y. Wang, T. Zhang, M. Kan, Y. Li, T. Wang and Y. Zhao, Joule (in press) [DOI: 10.1016/j.joule.2018.06.013].
29) K. Hamada, K. Yonezawa, K. Yamamoto, T. Taima, S. Hayase, N. Ooyagi, Y. Yamamoto, and K. Ohdaira, Ext. Abst. 2018 Int. Conf. Solid State Devices and Materials (SSDM2018), 2018, PS-6-10.
30) A.G. Dirks and H.J. Leamy, Thin Solid Films **47**, 219 (1977).

Figure Captions

Fig. 1. Surface SEM images of textured Si wafers.

Fig. 2. Optical reflectance spectra of textured and flat Si wafers.

Fig. 3. Cross-sectional SEM images of a PbI_2 film formed on textured Si by a solution method.

Fig. 4. Cross-sectional SEM images of $CsPbI_3$ layers deposited on the three types of textured wafers and on flat Si wafers.

Fig. 5. Optical reflectance spectra of three types of textured Si and flat Si coated with $CsPbI_3$ layers.

Fig. 6. Cross-sectional SEM images of sequentially-evaporated $CsI/PbI_2/Si$ stacks before annealing. (a) and (b) indicate underlying thin layers and columnar structures, respectively.

Fig. 7. Cross-sectional SEM and EDX mapping images of sequentially-evaporated $CsI/PbI_2/Si$ stacks before annealing and $CsPbI_3/Si$ stacks after annealing.

Fig. 8. Cross-sectional SEM and EDX mapping images of co-evaporated $(CsI)(PbI_2)/Si$ stacks before annealing and $CsPbI_3/Si$ stacks after annealing.

Table I. Etching conditions and pyramid heights.

Etchant	SE-2000H		SUN-X 600
Condition	90 °C, 15 min	90 °C, 60 min	70 °C, 50 min
Height (μm)	2.21±0.52	1.47±0.23	7.25±1.68
	[M]	[S]	[L]

Table II. R_{AVE} of flat and textured c-Si wafers in a wavelength region of 400–800 nm.

	Flat wafer	[S]	[M]	[L]
R_{AVE} (%)	24.5	11.8	9.9	12.8

Table III. R_{AVE} on $CsPbI_3$ layers formed on flat and textured c-Si wafers in a wavelength region of 400–800 nm.

	Flat wafer	S size	M size	L size
R_{AVE} (%)	16.5	6.6	6.2	6.0

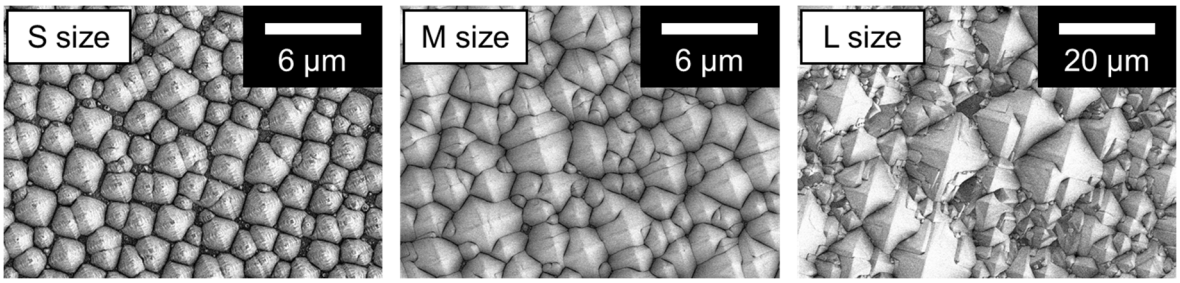

Fig.1. (Color Online) K. Hamada *et al.*

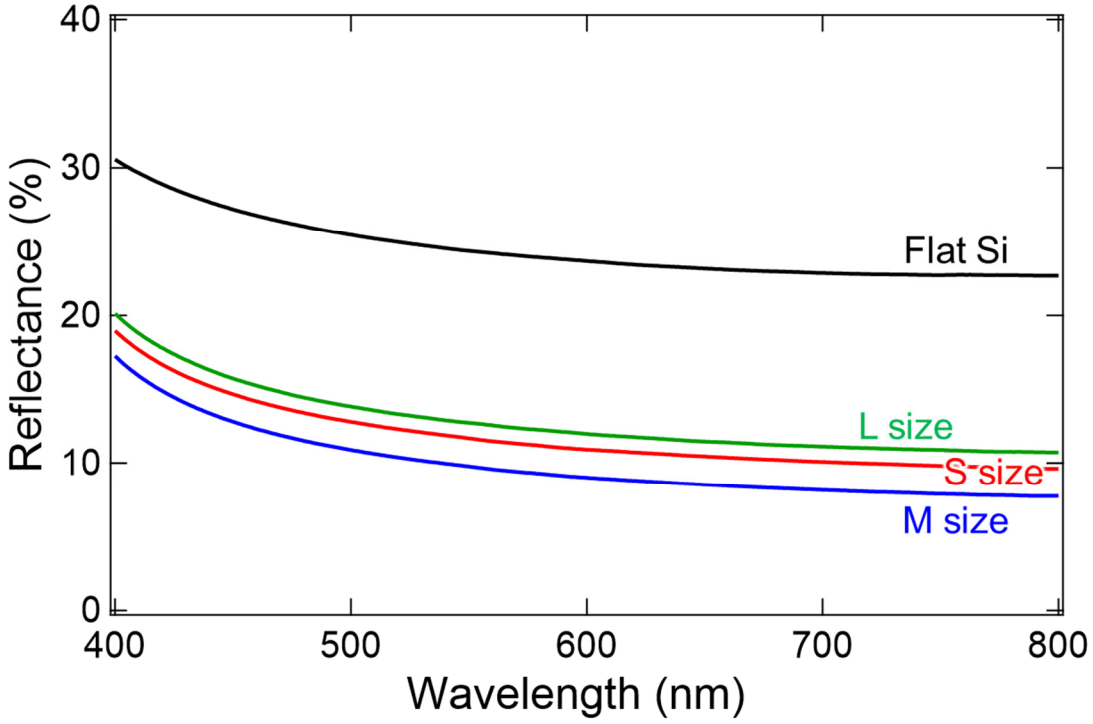

Fig. 2. (Color Online) K. Hamada *et al.*

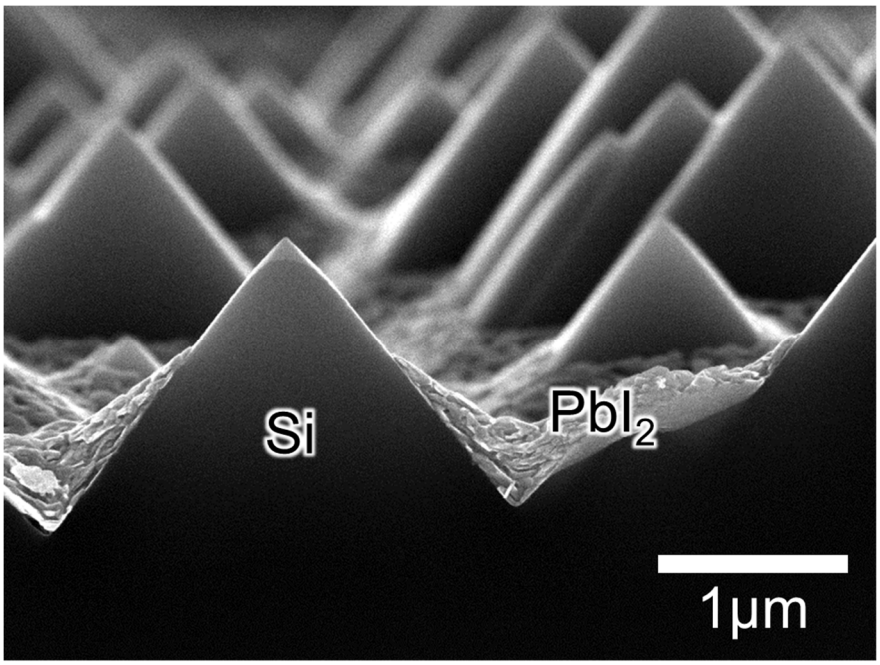

Fig. 3. (Color Online) K. Hamada *et al.*

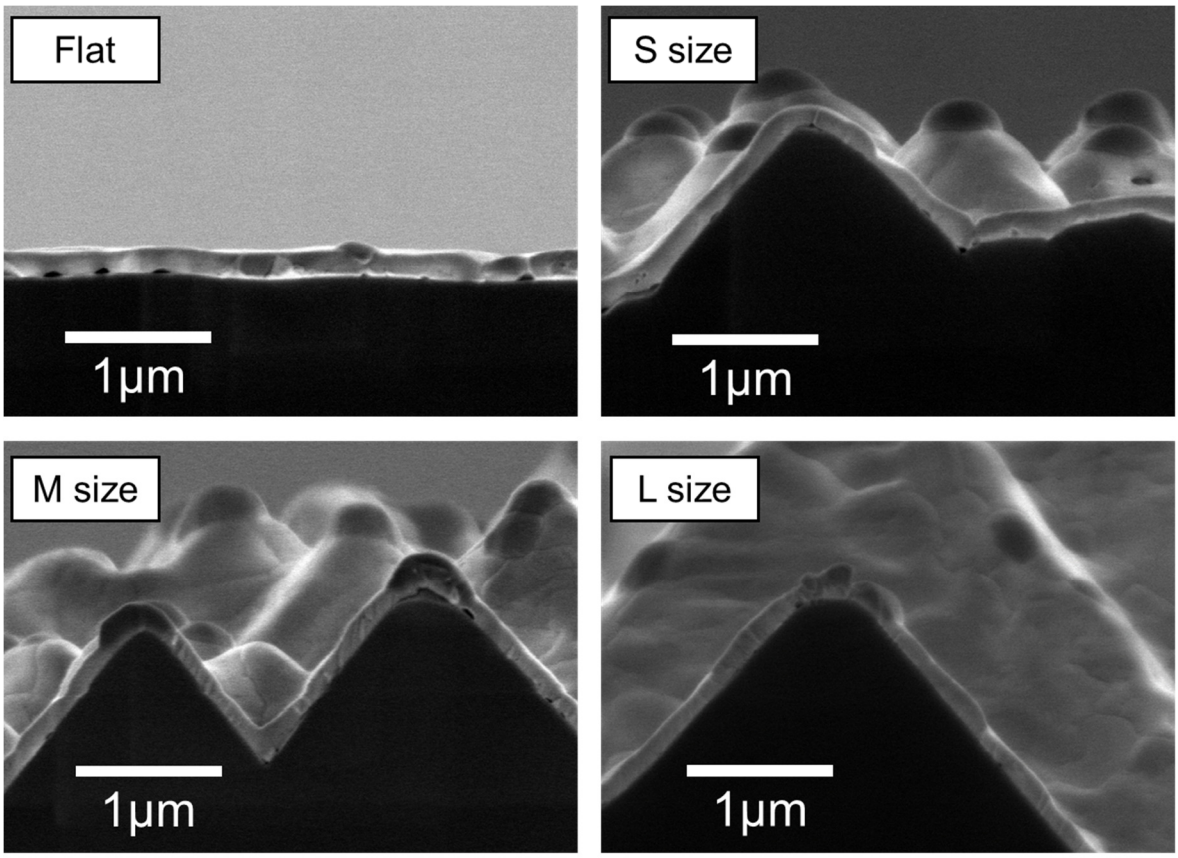

Fig. 4. (Color Online) K. Hamada *et al.*

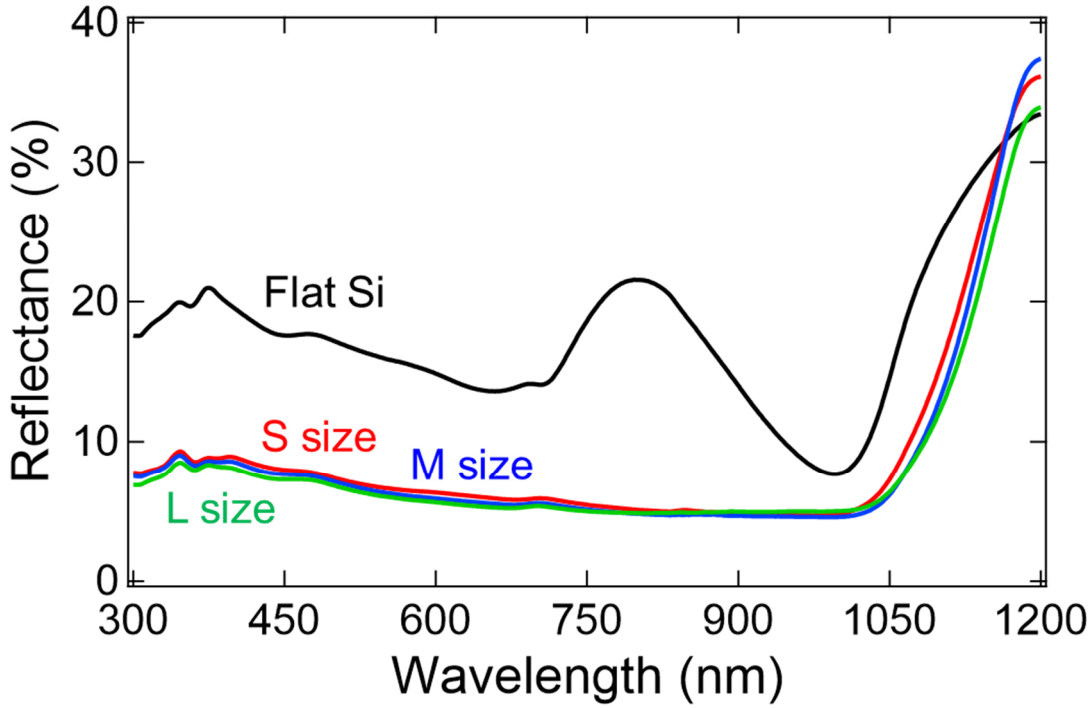

Fig. 5. (Color Online) K. Hamada *et al.*

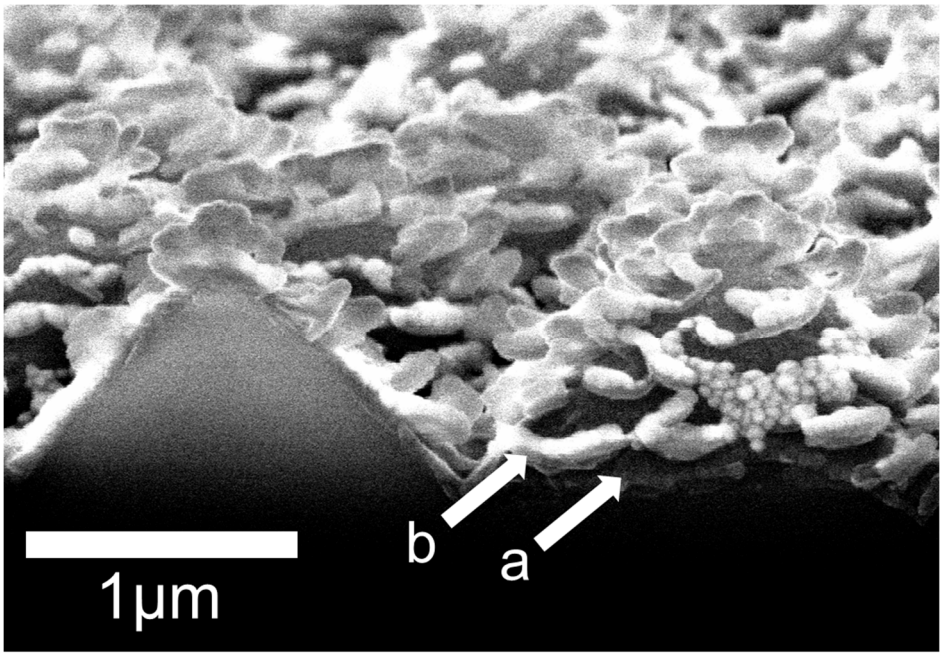

Fig. 6. (Color Online) K. Hamada *et al.*

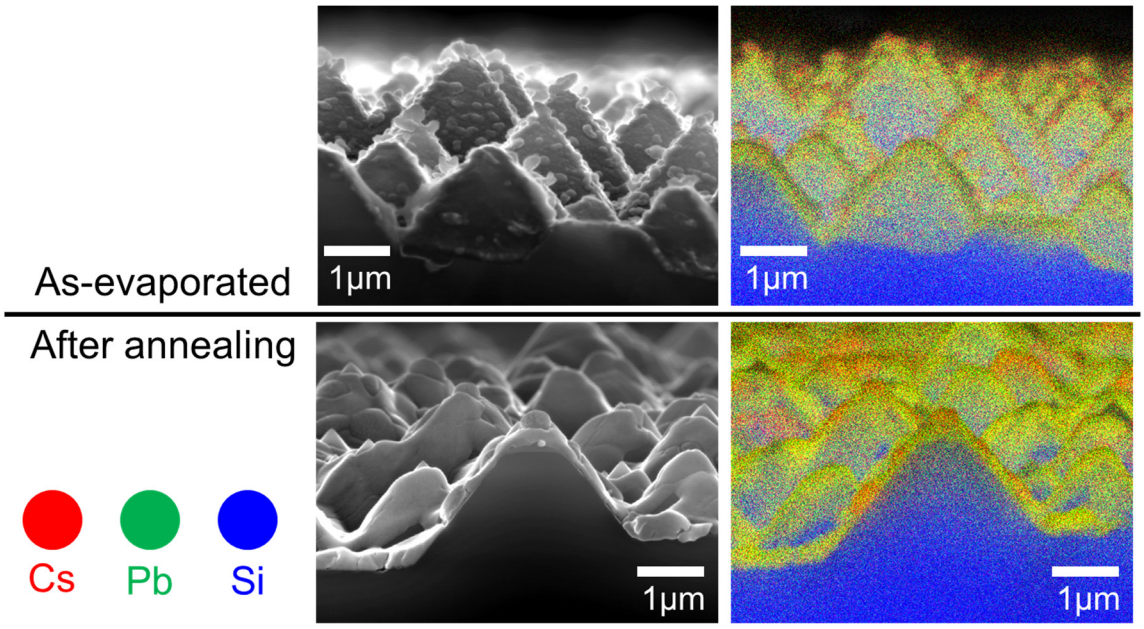

Fig. 7. (Color Online) K. Hamada *et al.*

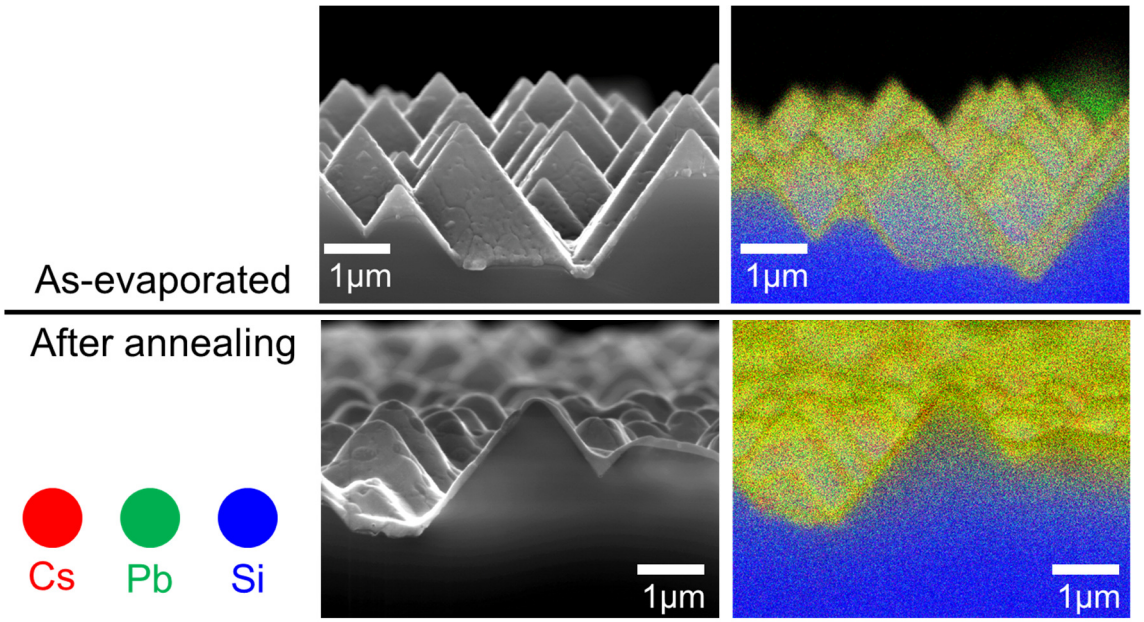

Fig. 8. (Color Online) K. Hamada *et al.*